Solar cycle variability of Mars dayside exospheric temperatures: Model evaluation of underlying thermal balances

S. W. Bougher,[1] T. M. McDunn,[1] K. A. Zoldak,[2] and J. M. Forbes[3]

Received 20 October 2008; revised 12 December 2008; accepted 9 January 2009; published 5 March 2009.

[1] The response of the Mars dayside exospheric temperatures to short and long term solar flux changes was recently established. Characterization of the relative importance of various thermospheric heating and cooling mechanisms for maintaining these Mars exospheric temperatures requires the systematic application of modern global dynamical models that capture both lower and upper atmosphere thermal and dynamical processes. Coupled Mars General Circulation Model (MGCM) plus Mars Thermospheric General Circulation Model (MTGCM) simulations are utilized for this study, closely matching conditions during Mars Global Surveyor drag measurements. Simulations confirm the major balance of EUV heating and thermal heat conduction at dayside exospheric altitudes. However, the influence of variable Martian global winds is significant and must be carefully considered when investigating the global regulation of Mars exospheric temperatures over the solar cycle and Martian seasons. Finally, the present MGCM-MTGCM heating and cooling processes suggests that an EUV-UV heating efficiency of 19% yields net heating in accord with MGS exospheric temperatures. **Citation:** Bougher, S. W., T. M. McDunn, K. A. Zoldak, and J. M. Forbes (2009), Solar cycle variability of Mars dayside exospheric temperatures: Model evaluation of underlying thermal balances, *Geophys. Res. Lett.*, *36*, L05201, doi:10.1029/2008GL036376.

1. Introduction

[2] Using densities derived from precise orbit determination of the Mars Global Surveyor (MGS) spacecraft from 1999 to mid-2005, the response of the Mars exosphere (both densities and temperatures) to short and long-term solar flux changes was recently established [*Forbes et al.*, 2006, 2008]. The MGS satellite was in a 93.7° inclination 1400–0200 LT sun-synchronous 370 × 437 km frozen orbit with periapsis confined to 40–60°S Latitude. The density and temperature values extracted represent averages over all longitudes, and are strongly biased towards dayside (LT = 1400) Southern Hemisphere conditions.

[3] The derived exospheric temperature is considered the thermal (cold) component as averaged over several species, but corresponding mostly to atomic oxygen. At MGS periapsis altitudes (near 370 km), thermal (cold) oxygen atoms are expected to dominate over non-thermal (hot) atoms over the Mars seasons and throughout the solar cycle [e.g., *Valeille et al.*, 2009; *Lichtenegger et al.*, 2006]. Thus, isothermal exospheric temperatures are assumed above the Mars exobase (~190 to 220 km) to MGS periapsis altitudes.

[4] The change in the derived exospheric temperatures (Texo) over the solar cycle is presented by *Forbes et al.* [2008]. These authors provide a least squared functional form of this solar cycle variation as follows:

$$Texo = 130.7 + 1.53 * F10.7 - 13.5 * \cos(Ls - 85) \quad (1)$$

[5] The first two terms in equation 1 capture the impact of the 81-day mean F10.7-cm fluxes received at Mars, thus taking into account the impact of changes in heliocentric distance with season. An additional small seasonal effect is included (Ls term) to account for solar declination changes and their impacts on local insolation.

[6] Figure 1 (green curve) illustrates the solar flux terms of this solar cycle variation, with the Ls effects removed. From Mars aphelion/solar minimum (MIN) to perihelion/solar maximum (MAX) conditions (F10.7 ~ 27 to 110), Texo varies from ~170 to 300°K. The slope of this Mars line is $\Delta T/\Delta F10.7 \sim 1.5$, which means that the exosphere temperature changes by 1.5°K per solar flux unit received at the planet. These temperatures are consistent with previously reported dayside exospheric values inferred from MGS Accelerometer (~200°K) [*Keating et al.*, 2007] and Mars Express (201 ± 10°K) [e.g., *LeBlanc et al.*, 2006] measurements obtained from mostly afternoon and non-polar locations for F10.7 ≤ 60. Other reported exospheric temperatures (≤240°K) derived from ionospheric peak plasma densities disagree with these MGS drag values for F10.7 > 70 [*Lichtenegger et al.*, 2006].

[7] Several processes determine Mars exospheric temperatures (cold component) and their variability [e.g., *Bougher et al.*, 1999]. These processes include: (1) solar EUV-UV fluxes producing heating, and its changes with solar cycle, solar rotation, distance from the sun, and local solar declination, (2) thermal heat conduction, (3) CO_2 15μm cooling, and (4) adiabatic heating and cooling associated with global dynamics. According to *Bougher et al.* [1999], the primary dayside balance occurs between EUV heating and thermal heat conduction, with CO_2 cooling playing a tertiary role. In addition, Mars adiabatic cooling, due to rising motions on the dayside from the global thermospheric circulation, should play a progressively more important role as the solar cycle advances. This "dynamical thermostat" cannot be ignored.

[8] Progress in the quantification of the relative importance of these heat balance mechanisms for maintaining Mars exospheric temperatures requires: (1) new measure-

[1]Atmospheric, Oceanic, and Space Sciences Department, University of Michigan, Ann Arbor, Michigan, USA.
[2]Department of Earth Sciences, California University of Pennsylvania, California, Pennsylvania, USA.
[3]Department of Aerospace Engineering Sciences, University of Colorado, Boulder, Colorado, USA.

0094-8276/09/2008GL036376

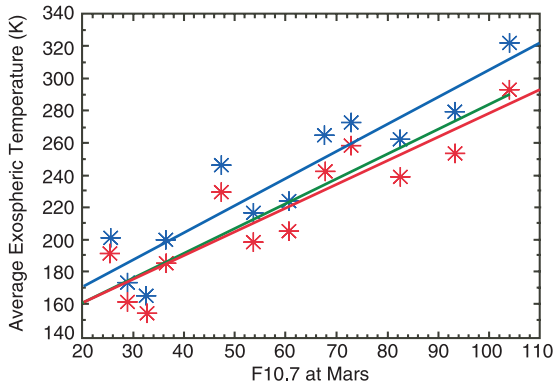

Figure 1. Simulated dayside exospheric temperatures over the solar cycle versus MGS drag temperatures. The green curve corresponds to the MGS mean solar cycle variation [*Forbes et al.*, 2008]. Blue (red) asterisks correspond to simulations using a 22% (19%) EUV-UV heating efficiency. The blue (red) curve corresponds to the linear least-squares-fit to the 22% (19%) model data-points.

ments of O-abundances in the Mars thermosphere for constraining CO_2 cooling rates, and (2) application of modern global dynamical models and comparison with recent datasets.

2. MGCM-MTGCM Formulation, Structure, Inputs

[9] Coupled Mars General Circulation Model (MGCM) plus Mars Thermospheric General Circulation Model (MTGCM) simulations are utilized for this study that closely match MGS drag sampling conditions.

[10] The MTGCM is a finite difference primitive equation model that self-consistently solves for time-dependent thermospheric neutral temperatures, neutral-ion densities, and neutral winds over the Mars globe. The modern MTGCM code [e.g., *Bougher et al.*, 2004, 2006; *Bell et al.*, 2007] contains time-evolving equations for the major neutral species (CO_2, CO, N_2, and O), selected minor neutral species (e.g., Ar, O_2), and several photochemically produced ions (e.g., O_2^+, CO_2^+ O^+, and NO^+) and electrons below 180 km. These composition, temperature, and 3-component wind fields are calculated on 33 pressure levels above 1.32 μbar, corresponding to altitudes from roughly 70 to 300 km (at solar maximum conditions), with a 5° resolution in latitude and longitude. The vertical coordinate is log pressure, with a vertical spacing of 0.5 scale heights. Key adjustable parameters which can be varied for MTGCM cases include the F10.7 or E10.7-cm index (solar EUV-UV flux variations over 2.4-225.0-nm), the heliocentric distance and solar declination corresponding to Mars seasons. A fast non-Local Thermodynamic Equilibrium (NLTE) 15-μm cooling scheme is currently implemented in the MTGCM, along with corresponding near-IR heating rates [e.g., *Bougher et al.*, 2006]. The feedback of simulated atomic O upon CO_2 cooling rates is important, and is included. These inputs are based upon recent detailed 1-D NLTE model calculations for the Mars atmosphere [e.g., *Lopez-Valverde et al.*, 1998].

[11] A detailed dayside photochemical ionosphere is formulated for the MTGCM [e.g., *Bougher et al.*, 2004]. Key ion-neutral reactions and rates are taken from modern 1-D ionospheric models [e.g., *Fox and Sung*, 2001]. This ionospheric formulation is critical to the self-consistent simulation of dayside atomic O abundances in the MTGCM. However, O abundances have never been directly measured for the Mars upper atmosphere, only inferred from UV airglow measurements [e.g., *Stewart et al.*, 1992]. This uncertainty in Mars O abundances directly impacts the simulation of CO_2 15μm cooling rates in the Mars upper atmosphere [e.g., *Huestis et al.*, 2008].

[12] The MTGCM is driven from below by the NASA Ames Mars MGCM code at the 1.32-μbar level (near 60–80 km) (see details by *Bougher et al.* [2004]). In other words, key variables are passed upward from the MGCM to the MTGCM at the 1.32-μbar level at every MTGCM grid point on 2-minute time steps: temperatures, zonal and meridional winds, and geopotential heights. This coupling allows both the migrating and non-migrating tides to cross the MTGCM lower boundary and the seasonal effects of the expansion and contraction of the Mars lower atmosphere to extend to the thermosphere. No downward coupling is presently activated between the MGCM and the MTGCM. However, the impact of lower atmosphere dynamics upon

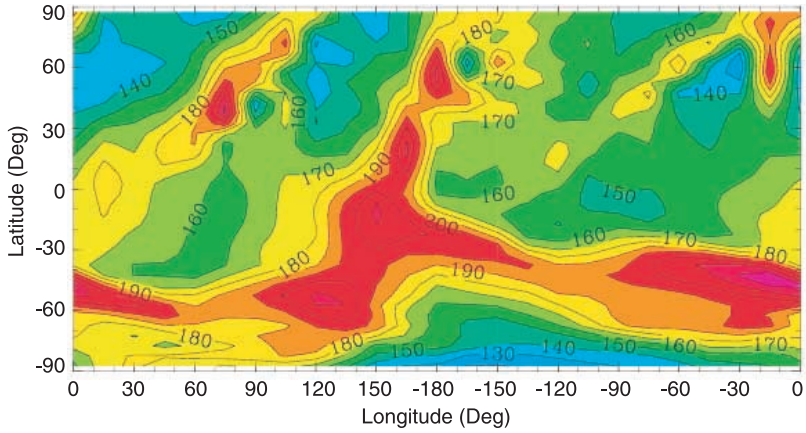

Figure 2. Simulated dayside (LT = 1400) exospheric temperature map for MIN (F10.7 = 25.5) conditions. Values range from a high of 240°K (Southern mid-latitudes) to a low of 140°K (Northern high latitudes). Temperature intervals are 10°K.

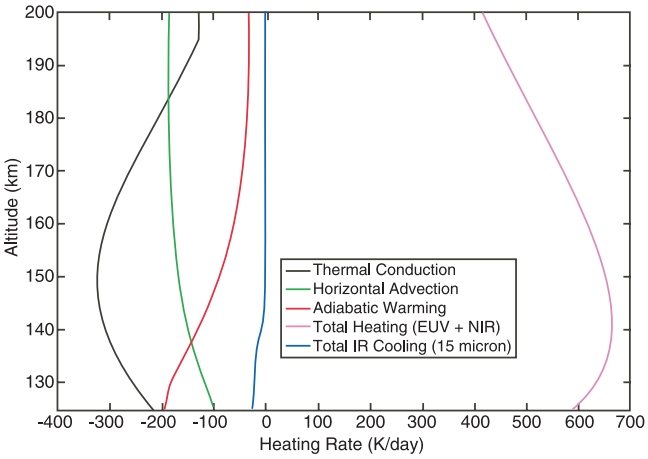

Figure 3. Simulated equatorial dayside heat balance terms (K/day) for MIN conditions. Curves are as follows: thermal conduction (black), EUV-UV heating (purple), CO_2 15-micron cooling (blue), adiabatic heating/cooling (red), hydrodynamic advection (green).

thermospheric densities and temperatures is significant [e.g., *Bell et al.*, 2007].

[13] For analyzing the present MGS drag datasets, the MGCM and MTGCM input parameters are now set as follows. F10.7 at Mars is varied from 25 to 104 units, corresponding to extreme MIN to MAX conditions. Solar EUV-UV heating is directly calculated (see details by *Bougher et al.* [1999]) utilizing an assumed heating efficiency of 22% or 19%, based upon detailed offline heating efficiency calculations (21 ± 2%) [*Fox et al.*, 1995; *Huestis et al.*, 2008]. Finally, the MGCM lower atmosphere horizontal dust distribution is adopted from MGS Thermal Emission Spectrometer mapping Year ♯1 [e.g., *Bell et al.*, 2007].

3. Results and Discussion

[14] Simulated exospheric temperatures are selected and organized to match the MGS drag dataset sampling conditions. For each coupled MGCM-MTGCM simulation, Texo values are collected at LT = 1400 over all longitudes spanning the 40–60°S latitude range. These values are averaged to remove longitude dependencies, in accord with the Mars exospheric temperatures plotted in Figure 1 (green curve). Twelve MGCM-MTGCM cases are examined initially (22% EUV-UV efficiency). Cases were chosen that span the full range of F10.7 at Mars, and also provide representative seasonal variations of solar declination. Specifically, equinox (Ls = 0 and 180) and solstice (Ls = 90 and 270) simulations were conducted for three levels of solar EUV-UV fluxes (low, medium and high) scaled to the seasonal Mars heliocentric distance.

[15] Figure 1 shows a comparison of MGS drag derived Texo values (green curve) over the solar cycle with simulated Texo values for these twelve cases (22% EUV-UV heating efficiency). A "best" match of model and data values would be seen if the blue asterisks evenly straddled the green curve from lower left to upper right. Equivalently, a least-squares-fit curve (blue) representing the model datapoints (blue asterisks) would overlap the green curve for a "best" fit. This does not occur, implying that the MGCM-MTGCM exospheric temperatures are too warm by 10 to 25°K from MIN to MAX conditions, respectively. The corresponding slope of the mean simulated Mars response is $\Delta T/\Delta F10.7 \sim 1.68$, 12% larger than observed.

[16] Alternatively, twelve additional MGCM-MTGCM cases were run for MIN to MAX conditions (red asterisks), now utilizing a 19% EUV-UV heating efficiency. A slight change in Texo occurs for MIN conditions (cooling by 10°K), while Texo for MAX conditions cools by 25–30°K. The near overlap of these observed (green curve) and modeled (red curve) Texo values over the solar cycle and Martian seasons is striking. The corresponding slope of the mean simulated Mars response is now $\Delta T/\Delta F10.7 \sim 1.45$. We can conclude that a ~19% heating efficiency, within the reasonable limits of detailed offline calculations [*Fox et al.*, 1995; *Huestis et al.*, 2008], provides an improved match of model and MGS observed dayside exospheric temperatures over the solar cycle and throughout all Martian seasons. For comparison, Laboratoire de Meteorologie Dynamique (LMD) MGCM simulations satisfactorily reproduce solar

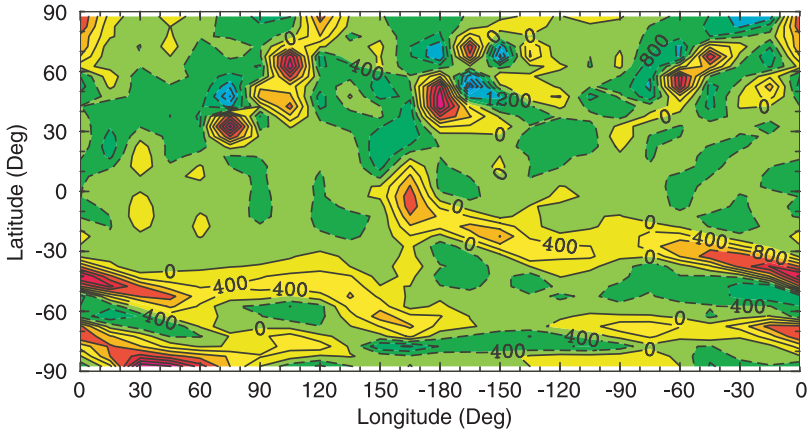

Figure 4. Simulated dayside adiabatic heating/cooling map at exospheric altitudes for MIN conditions. Values generally range from heating highs of +800 to 1500°K/day (Southern mid-latitudes) to cooling lows of −400 to −1200°K/day (Northern mid-latitudes). Contour intervals are 400°K/day (dashed lines: cooling; solid lines: heating).

cycle variations of dayside exospheric temperatures, but require an EUV-UV heating efficiency of 16%, lower than its theoretical value [*Gonzalez-Galindo et al.*, 2008]. Their CO_2 cooling rates (and associated atomic O abundances) may be smaller than corresponding MGCM-MTGCM values.

[17] What thermal balances are responsible for these MGCM-MTGCM simulated variations of dayside exospheric temperatures? Figure 2 shows a map of exospheric temperatures at LT = 1400 over all longitudes/latitudes for MIN conditions (EUV-UV efficiency of 19%). Notice cooler temperatures in Northern Hemisphere (summer) and equatorial latitudes, and warmer temperatures in Southern Hemisphere (winter) mid-latitudes (30–60°S). This temperature distribution is consistent with a summer-to-winter interhemispheric global circulation [e.g., *Bougher et al.*, 2006], providing adiabatic cooling in summer latitudes (upwelling), and adiabatic warming in winter latitudes (subsidence).

[18] Figure 3 illustrates heat balance terms for this same MIN simulation near the equator. The major balance occurs between EUV heating and thermal heat condition. CO_2 15-μm cooling effects are relatively small at all altitudes. This is consistent with the small O abundance calculated at the location of the mid-afternoon equatorial ionospheric peak (O/CO_2 ratio $\sim$ 0.7% at $\sim$116 km). However, adiabatic cooling and horizontal advection (resulting from local upwelling and diverging global winds) play a significant role in maintaining Texo.

[19] Variations of dynamical heating/cooling terms with longitude and latitude can be significant. Figure 4 shows a map of adiabatic heating/cooling rates corresponding to the temperature map of Figure 2. It is clear that a very close match of Northern Hemisphere cool temperatures and adiabatic cooling rates (upwelling winds) exists, along with Southern Hemisphere warm temperatures and adiabatic heating rates (subsiding winds). In general, this provides cooler Northern hemisphere (and warmer Southern hemisphere) aphelion temperatures than otherwise expected from radiative equilibrium considerations alone. In addition, a wave number 3 pattern of Northern Hemisphere "hot spots" (Figure 2) and adiabatic heating rates (Figure 4) is visible. These features are in accord with the high Northern latitude wave 3 non-migrating tidal structure observed in MGS Accelerometer and Radio Science datasets [e.g., *Bougher et al.*, 2004].

[20] Similar thermal balance effects are seen throughout the solar cycle. For MAX conditions, CO_2 15-μm cooling rates continue to be small, in accord with small O abundances calculated at the mid-afternoon equatorial ionospheric peak (O/CO_2 ratio $\sim$ 1.7% at $\sim$130 km). However, adiabatic cooling/heating rates intensify in concert with increasing inter- hemispheric winds as MAX conditions are approached. In particular, Southern Hemisphere adiabatic cooling rates approach -2500°K/day, while Northern hemisphere adiabatic heating rates can be nearly +3000°K/day. In short, the intensified perihelion inter-hemispheric circulation gives rise to adiabatic heating and cooling rates, nearly double those simulated for aphelion conditions [e.g., *Bougher et al.*, 2006].

[21] Finally, the MGCM-MTGCM simulations (19% efficiency) provide exospheric temperatures over the solar cycle ($\sim$192 to 294°K) that can be compared to corresponding temperatures at 150 km just above the ionospheric peak ($\sim$188 to 233°K). These latter values are similar to temperatures derived from Mars ionospheric peak plasma densities [e.g., *Lichtenegger et al.*, 2006]. However, MGCM-MTGCM simulations suggest that a further increase of thermospheric temperatures from 150 km to the exobase is likely.

[22] We conclude that the influence of Martian global winds must be carefully considered when investigating the thermal balances that regulate the solar cycle variation of Mars dayside exospheric temperatures [e.g., *Bougher et al.*, 1999]. Furthermore, even though CO_2 15-μm cooling is not a dominate factor in regulating Martian exospheric temperatures, its exact contribution cannot be accurately evaluated until directly measured atomic O abundances are available (e.g., future Mars Scout mission). Future work entails a systematic study of these thermal balances throughout the solar cycle and their dependence on tidal and gravity wave influences which impact global wind patterns.

[23] **Acknowledgments.** The NASA Mars Data Analysis Program (NNX07A084G) and the NSF ATM program (ATM-0535811) partially supported this research. Also, we are grateful to the National Center for Atmospheric Research for the use of supercomputer resources.

References

Bell, J. M., S. W. Bougher, and J. R. Murphy (2007), Vertical dust mixing and the interannual variations in the Mars thermosphere, *J. Geophys. Res.*, *112*, E12002, doi:10.1029/2006JE002856.

Bougher, S. W., S. Engel, R. G. Roble, and B. Foster (1999), Comparative terrestrial planet thermospheres: 2. Solar cycle variation of global structure and winds at equinox, *J. Geophys. Res.*, *104*, 16,591–16,611.

Bougher, S. W., S. Engel, D. P. Hinson, and J. R. Murphy (2004), MGS Radio Science electron density profiles: Interannual variability and implications for the Martian neutral atmosphere, *J. Geophys. Res.*, *109*, E03010, doi:10.1029/2003JE002154.

Bougher, S. W., J. M. Bell, J. R. Murphy, M. A. Lopez-Valverde, and P. G. Withers (2006), Polar warming in the Mars thermosphere: Seasonal variations owing to changing insolation and dust distributions, *Geophys. Res. Lett.*, *33*, L02203, doi:10.1029/2005GL024059.

Forbes, J. M., S. L. Bruinsma, and F. G. Lemoine (2006), Solar rotation effects in the thermospheres of Mars and Earth, *Science*, *312*, 1366–1368.

Forbes, J. M., F. G. Lemoine, S. L. Bruinsma, M. D. Smith, and X. Zhang (2008), Solar flux variability of Mars' exosphere densities and temperatures, *Geophys. Res. Lett.*, *35*, L01201, doi:10.1029/2007GL031904.

Fox, J. L., and K. Y. Sung (2001), Solar activity variations in the Venus ionosphere/thermosphere, *J. Geophys. Res.*, *106*, 21,305–21,335.

Fox, J. L., P. Zhou, and S. W. Bougher (1995), The Martian thermosphere/ionosphere at high and low solar activities, *Adv. Space Res.*, *17*, 203–218.

Gonzalez-Galindo, F., et al. (2008), The temperatures in the thermosphere as given by the LMD-MGCM: Variations and comparisons with data, paper presented at Mars Atmosphere: Modeling and Observations Workshop, NASA, Williamsburg, Va.

Huestis, D. L., et al. (2008), Cross sections and reaction rates for comparative planetary aeronomy, *Space Sci. Rev.*, *139*, 63–105, doi:10.1007/s11214-008-9383-7.

Keating, G. M., S. W. Bougher, M. E. Theriot, and R. H. Tolson (2007), Climatology of Mars thermosphere and exosphere temperatures, *EOS Trans., AGU*, *88*(52), Fall Meet. Suppl., Abstract P32A-02.

Leblanc, F., J. Y. Chaufray, J. Lilensten, O. Witasse, and J.-L. Bertaux (2006), Martian dayglow as seen by the SPICAM UV spectrograph on Mars Express, *J. Geophys. Res.*, *111*, E09S11, doi:10.1029/2005JE002664.

Lichtenegger, H. I. M., et al. (2006), Effects of low energetic neutral atoms on Martian and Venusian dayside exospheric temperature estimations, *Space Sci. Rev.*, *126*, 469–501, doi:10.1007/s11214-006-9082-1.

Lopez-Valverde, M. A., D. P. Edwards, M. Lopez-Puertas, and C. Roldan (1998), Non-local thermodynamic equilibrium in general circulation models of the Martian atmosphere: 1. Effects of the local thermodynamic equilibrium approximation on thermal cooling and solar heating, *J. Geophys. Res.*, *103*, 16,799–16,812.

Stewart, A. I. F., M. J. Alexander, R. R. Meier, L. J. Paxton, S. W. Bougher, and C. G. Fesen (1992), Atomic oxygen in the Martian thermosphere, *J. Geophys. Res.*, *97*, 91–102.

Valeille, A., et al. (2009), A study of suprathermal oxygen atoms in Mars upper thermosphere and exosphere over the range of limiting conditions, *Icarus*, doi:10.1016/j.icarus.2008.08.018, in press.

S. W. Bougher and T. M. McDunn, Atmospheric, Oceanic, and Space Sciences Department, University of Michigan, Space Research Building, Ann Arbor, MI 48109, USA. (bougher@umich.edu)

J. M. Forbes, Department of Aerospace Engineering Sciences, University of Colorado, Boulder, CO 80307, USA. (forbes@colorado.edu)

K. A. Zoldak, Department of Earth Sciences, California University of Pennsylvania, California, PA 15419, USA.